ACS APPLIED MATERIALS & INTERFACES

Research Article

www.acsami.org

Effect of Polyelectrolyte and Fatty Acid Soap on the Formation of $CaCO_3$ in the Bulk and the Deposit on Hard Surfaces

Hao Wang,[†,‡] Viveka Alfredsson,[‡] Juergen Tropsch,[§] Roland Ettl,[§] and Tommy Nylander*[,‡]

[†]State Key Laboratory of Coal Conversion, Institute of Coal Chemistry, Chinese Academy of Sciences, Taiyuan, Shanxi 030001, People's Republic of China

[‡]Physical Chemistry, Department of Chemistry, Lund University, PO Box 124, SE-221 00 Lund, Sweden

[§]BASF SE, 67056 Ludwigshafen, Germany

ABSTRACT: The effects of sodium polyacrylate (NaPAA) as well as potassium oleate on the nucleation and calcium carbonate crystal growth on hard surfaces, i.e., stainless steel and silica, have been investigated at different temperatures. The relation between the surface deposition and the corresponding bulk processes has been revealed by combining dynamic light scattering (DLS), scanning electron microscopy (SEM), X-ray diffraction (XRD), and ellipsometry. The aim was to further our understanding of the crystal deposition/growth mechanism and how it can be controlled by the presence of polyelectrolytes (NaPAA) or soap (potassium oleate). The addition of polyelectrolytes (NaPAA) or soap (potassium oleate) decreases the size of $CaCO_3$ particles in bulk solution and affects both crystal structure and morphology in the bulk as well as on hard surfaces. The amount of particles on hard surfaces decreases significantly in the presence of both potassium oleate and NaPAA. This was found to be a consequence of potassium oleate or NaPAA adsorption on the hard surface as well as on the $CaCO_3$ crystal surfaces. Here, the polymer NaPAA exhibited a stronger inhibition effect on the formation and growth of $CaCO_3$ particles than potassium oleate.

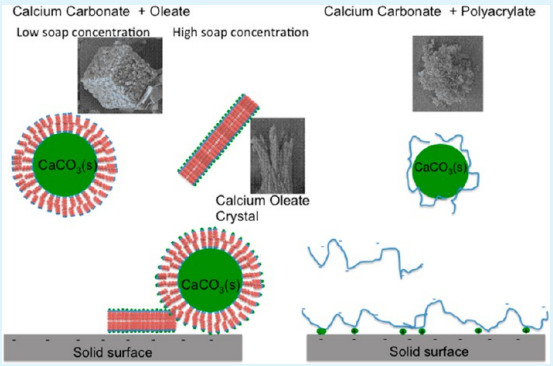

KEYWORDS: *calcium carbonate crystallization, potassium oleate, sodium acrylate, stainless steel surface, silica surface, crystal deposition, crystal growth*

1. INTRODUCTION

The control of calcium carbonate crystal formation in bulk and at interfaces is of key importance in nature and in applications.[1] Calcium carbonate is one of the most common type of minerals and is produced by a wide variety of biological organisms, which are able to exhibit exquisite control over the polymorph, location of nucleation, crystal size and shape, crystallographic orientation, composition, stability, and hierarchical assembly of the crystals.[2] Several different polymorphs of calcium carbonate have been identified, which in order of increasing solubility are calcite, aragonite, and vaterite (cf. refs 3 and 4). In excess of water, all of the polymorphs eventually transform into the most stable form, calcite. The less stable polymorphs may, however, be stabilized in the presence of additives. The classical nucleation theory is the most common approach to the describe the mechanism of the crystallization, as well as concepts such as spinodal decomposition and liquid−liquid demixing.[1] Recently, a prenucleation cluster pathway has been proposed.[1,5] Dissolved calcium carbonate has been shown under certain conditions to contain stable prenucleation ion clusters even if the solution is undersaturated. Such stable clusters have been proposed to be the relevant species for calcium carbonate nucleation sites. A stabilized form of amorphous calcium carbonate has been observed in bio-minerals.[6] It is clear that there is a wide interest in controlling the crystallization of $CaCO_3$, and therefore, various types of inorganic/organic additives have been used in order to control morphologies, crystal sizes, and polymorphs.[1,2]

Particle morphology as well as the polymorph of inorganic materials can be controlled by applying aqueous soluble additives, such as surfactants or polymers.[7,8] It is well-known that surfactants can influence several crystallization steps, including nucleation and crystal growth and aggregation, and as a consequence, can control the formation of various crystal phases. Surfactant aggregates have also been used as micro-reactors for preparation of specific morphologies, sizes, or new crystal structures of inorganic[9,10] or organic[11] materials. In addition, surfactants are used widely as templates to control the crystal size distribution and habit of the crystallization.[12−15] Potassium oleate is one of the common surface-active components used in industrial applications like flotation or other processes involving an agglomeration process, but it is also of importance in ADW (automatic dishwasher) processes.[16] In the ADW application, the high soap

Received: May 28, 2015
Accepted: September 10, 2015
Published: September 10, 2015

DOI: 10.1021/acsami.5b04679
ACS Appl. Mater. Interfaces 2015, 7, 21115−21129

concentration corresponds to the cleaning of greasy dishes, where the soap is formed from the hydrolyses of triglycerides at high pH. Antti and Forssberg[17] has found that oleate at low concentration adsorbs as a monolayer and at increased concentration precipitates at high pH in the presence calcite, while a bilayer is formed on apatite. Lu et al. compared the differences in adsorption of oleate on fluorite, apatite, and calcite, respectively. They found that adsorption was dependent on differences in calcium site density and mineral solubility.[18] Apatite monolayer adsorption occurred at low temperature, but surface precipitation of calcium oleate was predominant at 65 °C, pH 9.5. The adsorption density prior to monolayer coverage on the three studied surfaces follows the order fluorite > calcite > apatite; i.e., it scales with the calcium surface site density. Beyond monolayer coverage, the adsorption density follows the order of solubility of the minerals, that is, calcite > fluorite > apatite. Interestingly, force measurements using a colloid probe AFM have revealed a strong attractive force between calcium dioleate colloidal probe and a fluorite surface, whereas the corresponding interactions with a calcite surface was found to be repulsive.[19,20] These results were attributed to hydrophobic interaction between the probe and the fluorite surface. Somasundaran described a strong synergistic effect when oleate and starch are used together as additives promoting adsorption of both.[21] Although nucleation and growth mechanisms, as well as the kinetics of calcium carbonates formation in the presence of surfactants, have previously been studied, significantly less is known about the $CaCO_3$ crystal formation/deposition mechanism on a solid surface.

Synthetic polymers have also been used to control calcium carbonate growth. In some cases, simple anionic polymers, such as poly(acrylic acid), poly(acrylonitrile), and poly(styrenesulfonate), which can inhibit crystallization in bulk, have been used to prevent limescale formation in boilers, water pipes, and dishes and cutlery in the automatic dish washers.[22−24] Naka et al.[25] observed that vaterite is stabilized by the addition of poly(acrylic acid). Either spherical or nanoparticulate morpohologies are formed, depending on when during the crystallization the polymer is added. Wang et al.[26] proposed a mechanism based on so-called mesocrystals that could explain peculiar shapes of $CaCO_3$ crystals formed in the presence of polystyrenesulfonate. They deduced that the polymer affected the process by complexing ions and therefore reducing nucleation as well as by stabilizing intermediate amorphous particles and controlling the assembly of the mesocrystals. Loy et al.[27] studied the influences of concentration and molecular weight of poly(acrylic acid) sodium on the inhibition of $CaCO_3$ formation. They found that nucleation temperature is strongly dependent on the molecular weight distribution of the sodium polyacrylate (NaPAA) and high molecular weight species govern the inhibition under competitive adsorption conditions. Abdel-Aal and Sawada[28] concluded that the inhibition of the $CaCO_3$ adhesion process is attributed to the adsorption of the polymer on the growing calcite adhered on the solid (gold) surface, and the presence of the inhibitor causes deformation of the crystal morphology of both the adhered and precipitated crystals. Even though a wide variety of soluble organic additives were examined for their effects on the crystallization of $CaCO_3$,[1,29−33] the mechanisms by which these organic additives affect nucleation and growth of calcium carbonate are not yet fully understood. Gebauer et al. found that the poly(acrylic acid) (PAA) binding capacity for free calcium ions is too low to explain the prevention of calcium carbonate particle nucleation.[34] Consequently, they concluded that the PAA calcium-ion binding capacity is not the main reason for the inhibition of nucleation. Instead, they argue that adsorption of the prenucleation-stage equilibrium clusters to PAA stabilizes them against aggregation and thereby prevents nucleation.

The relationship between bulk precipitation and surface $CaCO_3$ formation in the presence of polymer and surfactant has so far not received sufficient attention. In particular, there is a lack of knowledge on how the temperature affects the $CaCO_3$ deposition under these conditions.

The aim of this study is to reveal the effect of surfactants or polymers on the formation and transformation processes of calcium carbonate deposits on different hard surfaces in relation to precipitation in the bulk solution. This will provide the necessary knowledge to develop processes and detergents that give reduce calcium carbonate deposition. Here, we have chosen to study the effect of K-oleate and NaPAA at pH 10 under different temperatures, which are typical components and conditions during a typical ADW wash cycle. Furthermore, the effect of surface properties on the process was determined. Three types of surfaces were used: smooth silicon wafers, with average roughness <1 nm, that were either acid cleaned (fewer deprotonated OH groups) or alkaline treated (with larger negative charge),[35] and a stainless steel surface with an average surface roughness of 30 nm[36] but also with an isoelectric point close to silica at pH between 3 and 4.[37,38] The larger roughness is expected to provide a large effective surface area and more nucleation sites for the crystal formation on the surface. A null ellipsometer was used to in situ follow the adsorption kinetics and adsorbed amount of $CaCO_3$ particles on the surface. The particles were characterized with scanning electron microscopy (SEM), atomic force microscopy (AFM), and X-ray diffraction (XRD).

2. EXPERIMENTAL SECTION

2.1. Preparation of $CaCO_3$ Crystals from Hard Water in the Presence of Surfactant and Polymer. The following chemicals were used without further purification: $CaCl_2$ (Sigma-Aldrich), $MgCl_2$ (anhydrous, >98%) (Sigma-Aldrich), $NaHCO_3$ (Merck, >99.5%), Na_2CO_3 (Sigma-Aldrich, >99%), and potassium oleate (K-oleate) (M_w = 320.55g/mol) (TCI). Poly(sodium acrylate) (NaPAA, M_w = 8000) was provided by BASF. Milli-Q water was used for the preparation of the hard water and other aqueous solutions. Hard water (21° dH) was prepared by adding 4 mM Ca^{2+}/Mg^{2+} (4:1) + 8 mM HCO_3^- to water and setting the pH to 10 by using Na_2CO_3. For this purpose, stock solutions of $CaCl_2$, $MgCl_2$, $NaHCO_3$, and Na_2CO_3 with concentrations of 0.5, 0.1, 0.5, and 1.0 M, respectively, were used. $CaCO_3$ crystals were precipitated from solution by fast addition of the concentrated stock solutions of $NaHCO_3$ and Na_2CO_3 as well as additives (surfactant or polymer) to the desired final concentrations, into a beaker containing aqueous solutions of 4 mM $CaCl_2$ and $MgCl_2$ (4:1 molar ratio) at two reaction temperatures of 25 ± 0.2 and 55 ± 0.2 °C, respectively. The temperature was controlled by using a water bath. During mixing, pH adjustments, and crystal formation/growth, the solution was stirred at a constant rate of 300 rpm using a magnetic stirrer bar.

2.2. Surface Preparation and Treatment. The three types of surfaces chosen as substrates for the deposition experiments were a stainless steel surface (304), an acid treated silica surface, and an alkali treated silica surface. The silica surfaces (p-type, boron doped) were thermally oxidized in an oxygen atmosphere at 920 °C for 1 h, followed by annealing and cooling in an argon flow. This procedure yields a 300 Å thick SiO_2 and significantly increases the sensitivity of the ellipsometry measurements.[39] The oxidized wafers were cleaned in

DOI: 10.1021/acsami.5b04679
ACS Appl. Mater. Interfaces 2015, 7, 21115−21129

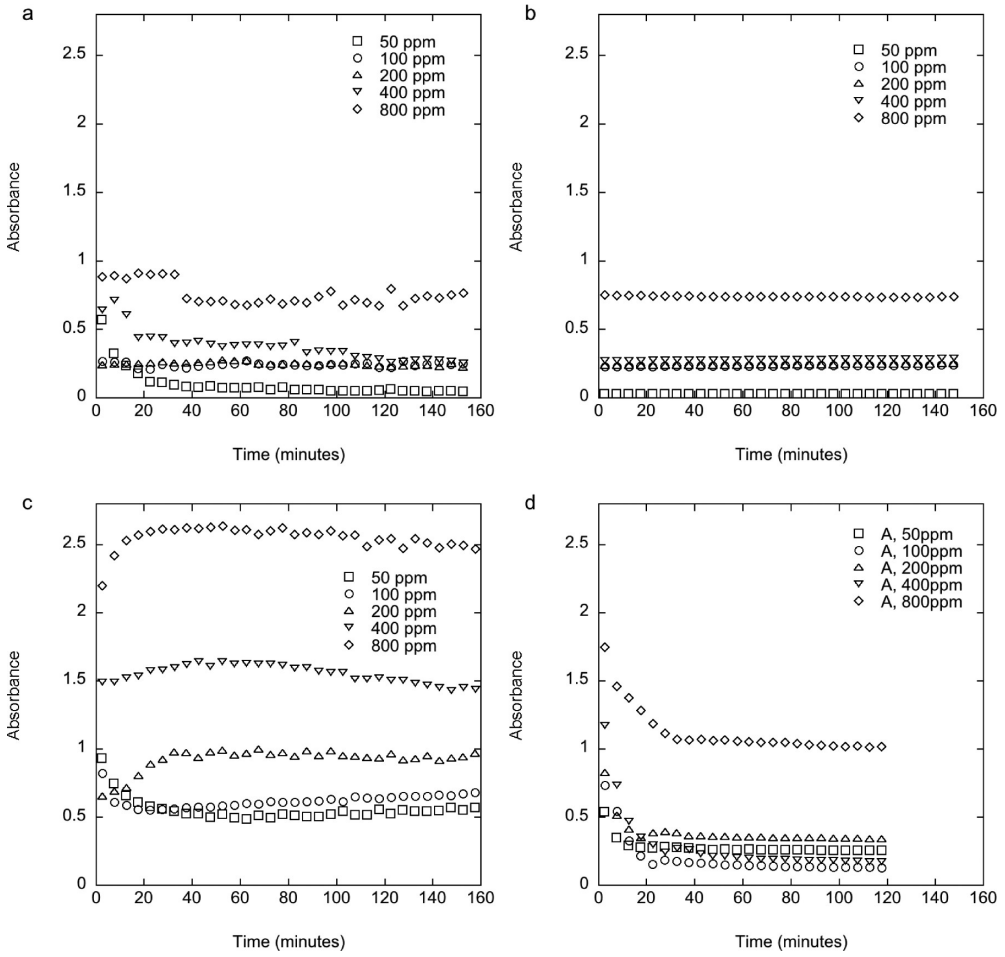

Figure 1. Turbidity (shown as absorbance) caused by $CaCO_3$ precipitation from hard water as a function of time at different oleate concentrations and temperatures: 55 °C (a and b) and 25 °C (c and d), pH = 10. The data is recorded with agitation (a, c) and after the agitation was stopped (b, d). For the sake of clarity, only every tenth recorded data point is shown in the graph.

a mixture of (1) 25% NH_4OH, 30% H_2O_2, and water (1:1:5 by volume) at 80 °C, (2) followed by boiling for 10 min in a mixture of concentrated hydrochloric acid, 30% H_2O_2, and water (1:1:5 by volume) at 80 °C for the acid treated silica wafer and, for the alkali treated silica wafer, an additional alkaline step (2) was added. Finally, the cleaned oxidized wafers were stored in ethanol before use. The stainless steel surfaces were cleaned by using the alkali detergent, Decon 90, at a concentration of 2 wt % and thoroughly rinsing with water. The $CaCO_3$ deposition from hard water was achieved by immersing the silica or stainless steel plate into water with a horizontal (surface subject to sedimentation) orientation. The stock solution of concentrated $NaHCO_3$, Na_2CO_3, and additives were then quickly added under identical conditions as was used for following the bulk precipitation/crystallization. The sample was taken out of the solution after 1 h of equilibration time and rinsed with purified water to remove any residual salt solution. The plate with the deposit was then dried in a closed, dust-free container.

2.3. Experimental Methods. An automated Rudolph Research thin-film null Ellipsometer, type 43603-200E, was used to measure (in situ) the adsorbed amount and the thickness of the adsorbed layers. It should be noted that we could not follow the adsorption of $CaCO_3$ particles by ellipsometry under the employed conditions with sufficient accuracy as the adsorbed amount of $CaCO_3$ alone is too low and the deposition was inhomogeneously distributed on the surface. We therefore only used ellipsometry to follow the adsorption of $CaCO_3$ particles in the presence of polymer on the surface, which gave sufficient surface coverage as was also apparent from the SEM and AFM images. We also attempted to study the $CaCO_3$ adsorption in the presence of oleate, but the high turbidity of the solution made ellipsometry measurements too challenging to follow the kinetics of the process. Ellipsometry is based on measurements of the change in the state of polarization of light in terms of the relative phase shift, Δ, and the relative change in amplitude, Ψ, upon reflection against an interface.[40] On the basis of these data and the measured optical properties of the substrate, the refractive index, n_f, and the film thickness, d_f, of the deposited layer can be determined.[41,42] The approach used to determine the properties of the used silicon substrate with a 300 Å thick oxide layer is described by Landgren and Joensson.[39] The adsorbed amount was calculated using the formula of de Feijter et al:[43]

$$\Gamma = \frac{d_f(n_f - n_0)}{dn/dc}$$

Here, n_0 is the refractive index of the ambient bulk solution and dn/dc is the refractive index increment of the adsorbing substance, where a value of 0.15 was used as described in previous studies[44−46] for polymer layers. The data from ellipsometry measurements is evaluated assuming a homogeneous layer. Therefore, the thickness extracted from such a model represents an optical average thickness, which does not necessary represent the physical thickness of the adsorbed layer in particular at low surface coverage. All measurements were performed at a wavelength of 401.5 nm and an angle of incidence of 68.5°. A 5 mL thermostated cuvette was used for the in situ measurements at 25.0 °C or other temperatures. The solution in the cuvette was agitated with a magnetic stirrer at about 300 rpm.

The deposited $CaCO_3$ particles were characterized by SEM (JEOL JSM-6700F), X-ray diffraction (XRD), and AFM (Digital Instruments,

DOI: 10.1021/acsami.5b04679
ACS Appl. Mater. Interfaces 2015, 7, 21115−21129

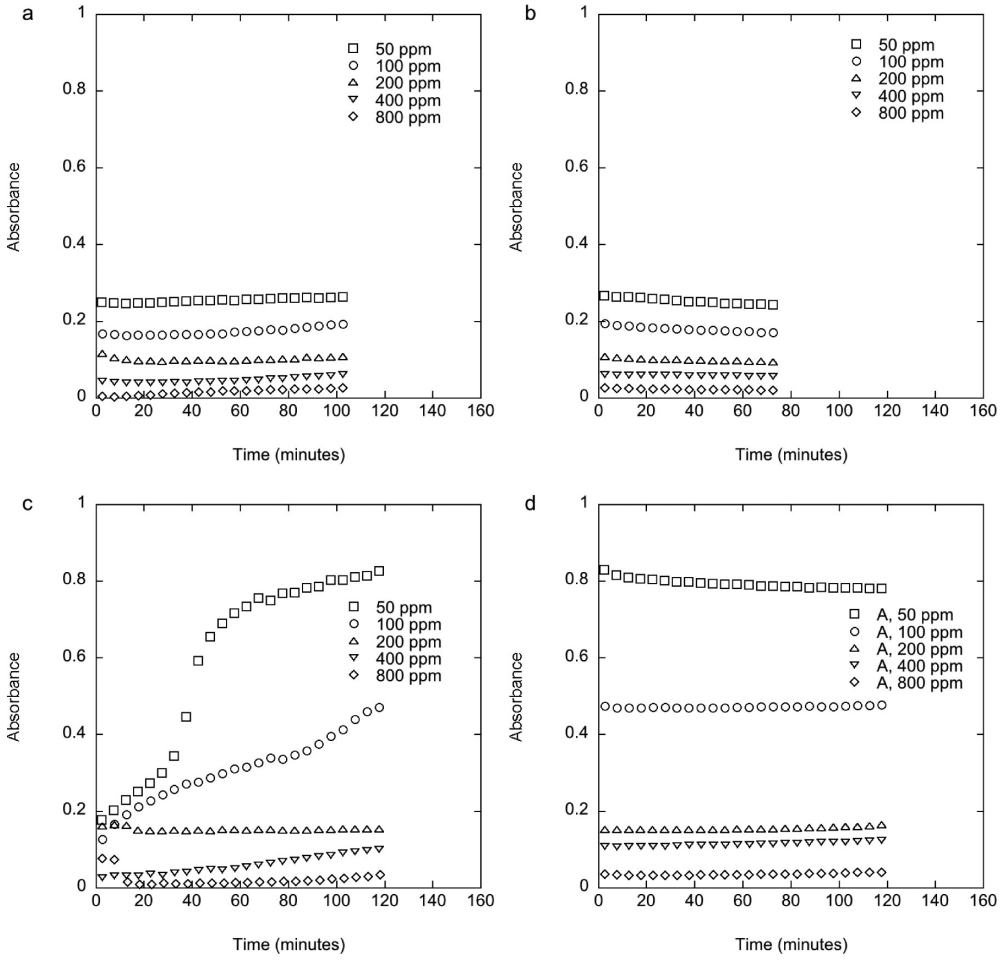

Figure 2. Turbidity (shown as absorbance) caused by $CaCO_3$ precipitation from hard water as a function of time with different NaPAA concentrations at 25 °C (a and b) and 55 °C (c and d), pH = 10. The data is recorded with agitation (a, c) and after the agitation was stopped (b, d). For the sake of clarity, only every tenth recorded data point is shown in the graph.

Nanoscope III, tapping mode). All samples were Au-coated prior to being examined by the SEM. The SEM was fitted with a field emission source and operated at an accelerating voltage of 5.0 kV. The XRD measurements were conducted using a Rigaku D/max-2400 powder X-ray diffractometer with Cu Kα radiation (40 kV, 120 mA), and 0.02 step and 2θ range of 20−60° were selected to analyze the crystal structure and type. The X-ray diffraction peaks at 2θ = 29.4°, 26.2°, and 27.0° for calcite (104), aragonite (111), and vaterite (112), respectively, were used to calculate the polymorphic ratio of the polymorphs in the precipitated $CaCO_3$.

Surface tension measurements were carried out using a Tensionmeter (K6, KRÜSS GmbH, Germany) to determine the CMC of K-oleate. During the measurement, the Platinum−Iridium ring was used.

The bulk precipitation/crystallization kinetics in the reaction mixture was characterized by comparing the scattering from dispersion, i.e., the turbidity, without sedimentation, that is, with stirring to capture the crystal/particle growth process, as well as after the agitation had stopped to capture the sedimentation process. For this purpose, an UV/vis Spectrometer (PerkinElmer LS-50B spectrometer) at a wavelength of 500 nm was used.

Quantitative information about formed particles was obtained by dynamic light scattering (DLS) to characterize the supernatant and scanning electron microscopy (SEM) for the precipitate. For DLS measurement, the reaction solution with particles was prepared with agitation and then equilibrated for 15 min without agitation. This means that the large particles have sedimented to the bottom of the reaction vessel during this process. The supernatant, characterized by DLS, only contained the small and colloidally stable particles, that contributed to the scattering. The DLS data also confirms that the particles in the supernatant are finely dispersed with particle sizes of only a few hundred nanometers and a rather narrow size distribution. However, for SEM measurements, the precipitate was collected by centrifugation (5000 rpm and 10 min), followed by filtration using a glass filter funnel (porosity of 0.45 μm). The particles were subsequently rinsed three times with Milli-Q water and then dried in the oven at 50 °C for at least 24 h. Thus, the SEM images show only the large particles from the sediment, which also have a large polydispersity.

3. RESULTS

3.1. Kinetics of $CaCO_3$ Bulk Precipitation in the Presence of K-oleate and NaPAA. We first performed turbidity measurements to map the effect of the surfactant and polymer concentrations as a function of time. It is important to note that any change in turbidity reflects formation, growth, and aggregation of the particle as well as precipitation and sedimentation. The latter process is expected to lead to a decrease in turbidity, while the other processes are expected to lead to an increase in turbidity.

The turbidity of solutions at 55 °C remained high immediately after adding Na_2CO_3 stock solution during agitation (Figure 1a). The turbidity, measured as absorbance, initially decreased steeply with time for the different concentrations of oleate as the precipitate settled in the cuvette. This effect is most pronounced for the lowest

DOI: 10.1021/acsami.5b04679
ACS Appl. Mater. Interfaces 2015, 7, 21115−21129

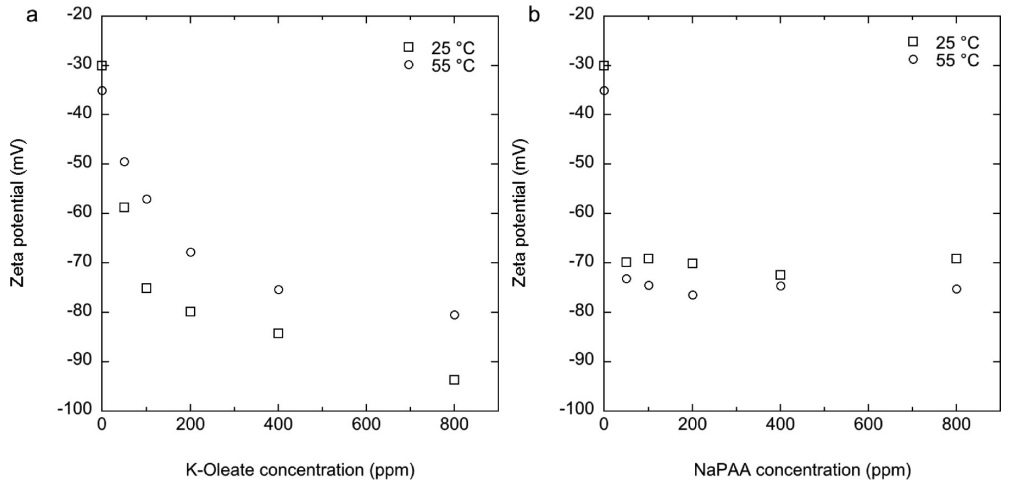

Figure 3. Variation of the zeta potential of $CaCO_3$ precipitate formed at 25 and 55 °C as a function of polyelectrolyte concentrations. (a) K-oleate; (b) NaPAA at pH = 10.

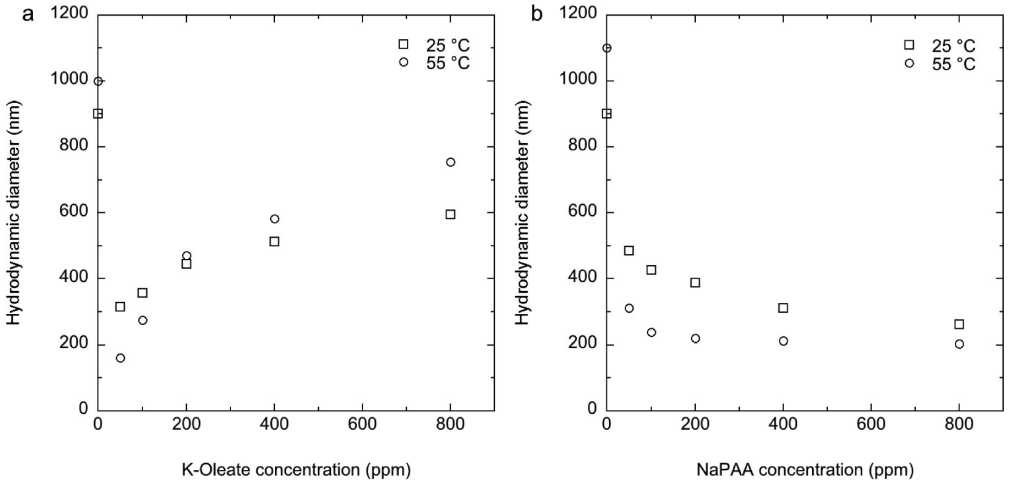

Figure 4. Size, i.e., the hydrodynamic diameter determined by DLS, of $CaCO_3$ particle formed at 25 and 55 °C as a function of concentration of additives. (a) K-oleate; (b) NaPAA. The pH = 10.

concentration of K-oleate. The turbidity reaches a low steady-state value already after about 20 min, which shows that most of the precipitate from the solution will settle fast. Furthermore, the turbidity remained constant and no further sedimentation of particles from the solution occurred even if the agitation was stopped after 160 min (Figure 1b). The steady-state value of the turbidity of the solution increased systematically with increasing concentration of the oleate. This indicates that there are more and/or larger Ca-oleate/$CaCO_3$ particles dispersed in the solution at higher concentration of soap even after sedimentation.

The corresponding results recorded at 25 °C (Figure 1c,d) are quite different from those at 55 °C (Figure 1a,b). The turbidity versus time at 25 °C appears to have an inflection point (Figure 1c), which again reflects the competition between the sedimentation and the aggregation processes. For the lower oleate concentrations (50 and 100 ppm), the turbidity initially decreased steeply with time as the precipitate settled in the cuvette. Eventually, after about 20 min, the turbidity reaches a low steady-state value, which shows that most of the precipitate has sedimented. However, for the higher oleate concentrations, the turbidity of the solution initially increases with time and increased with concentration of oleate in the solution until a plateau is observed after 20 min. When agitation of the solution is stopped, sedimentation leads to a steep decrease in turbidity during the initial 20 min after which it approached steady state (Figure 1d).

The turbidity of the solution in the presence of NaPAA at 25 °C remained constant after a slight decrease in turbidity during the initial stage (Figure 2a). The turbidity of solution decreased drastically with increasing polymer concentration. Furthermore, the turbidity still remained constant for a long time even when the agitation was stopped, and very few particles were observed to sediment to the bottom of the cuvette (Figure 2b). The turbidity after adding 50 ppm of NaPAA at 55 °C initially increases slowly followed by a steeper increase after 30 min, Figure 2c. After about 50 min, the increase in turbidity levels off and eventually a plateau value is reached. This behavior can possibly be attributed to the effect of polymer adsorption on the particle surface. When the number of particles increases, there is not a sufficient amount of polymer to prevent the particle growth, but when $CaCO_3$ content decreases below saturation limit, the particle growth reaches a plateau value. This is consistent with the observation that, at a polymer concentration of 200 ppm and above, the turbidity of the solution remains almost constant indicating that the particle

DOI: 10.1021/acsami.5b04679
ACS Appl. Mater. Interfaces 2015, 7, 21115−21129

growth is inhibited. We also note that, as the NaPAA concentration increases, the turbidity of solution steeply decreases and, when the concentration of NaPAA reaches 800 ppm, the turbidity is close to zero. This suggests inhibition of nucleation. When the agitation is stopped after 2 h (Figure 2d), the change in turbidity is minute indicating that no further particle growth or sedimentation occurs. We can conclude that the polymer NaPAA is more efficient than the K-oleate in preventing the formation and growth of $CaCO_3$ crystals

3.2. Properties of Dispersed $CaCO_3$ Particles Formed in the Presence of K-oleate and NaPAA. It is well-known that polyelectrolytes, such as NaPAA, as well as surfactants like K-oleate potentially can adsorb on surfaces of $CaCO_3$ crystals and thereby significantly affect the crystal surface charge and size. Above, we discussed the kinetics of the particle formation and growth and we were able to establish when the process reached steady state. We here discuss the properties of the dispersed particles at steady state. The properties of the larger sedimented particles are discussed in Section 3.3.

The effects of K-oleate and NaPAA concentration on the surface charge and size of $CaCO_3$ particles were studied using zeta potential and DLS measurements at 25 and 55 °C (Figures 3 and 4). We here note that the measurements are performed for the mixture, and hence, the absolute value of the zeta potential is more negative than one would expect for isolated $CaCO_3$ crystals. The rational for performing the measurements on the whole mixture is that the solid surfaces are exposed to this dispersion. Isolation of the separation of the crystals is likely to perturb the system. The critical micelle concentration (CMC) for K-oleate was first determined to be about 300 ppm (0.94 mM) by surface tension measurements (data not shown), which is in accordance with the value of 0.9−1.0 mM reported by Klevens.[47] The temperature was found to have little influence on the surface tension and CMC under the applied conditions. The zeta potential measurements (Figure 3a) show that $CaCO_3$ particles are negatively charged in the absence of K-oleate and the surface charge gradually becomes more negative with increasing K-oleate concentration. The particle size also increases with the K-oleate concentration (Figure 4a). These observations are attributed to the binding of oleate ion to the $CaCO_3$ particle surface. Furthermore, this interaction causes an exchange between the oleate ions and carbonate ions on the surface of $CaCO_3$ according to the chemical reaction scheme (1a−1c):

$$CaCO_3(s) \leftrightharpoons Ca^{2+} + CO_3^{2-} \quad (1a)$$

$$CaCO_3(s) + CO_2(aq) + H_2O(l) \leftrightharpoons Ca^{2+}(aq) + 2HCO_3^{-}(aq) \quad (1b)$$

$$2C_{17}H_{35}COO^{-}(aq) + Ca^{2+}(aq) \leftrightharpoons (C_{17}H_{35}COO)_2Ca(s) \quad (1c)$$

Ca-oleate is water insoluble and remains on the $CaCO_3$ surface, indicated by (s). Note that the solubilization of $CaCO_3$ is facilitated by dissolved CO_2 in the aqueous phase according to 1b. Lu et al. have shown using infrared that the surface layer structure is composed by oleic acid, chemisorbed oleate, and surface precipitated calcium dioleate.[18] At pH 8.0, oleic acid was found to be the dominating specie, while at pH 9.5, chemisorbed oleate dominates at low fatty acid concentration. The major specie at higher concentration is surface precipitated calcium dioleate. Chemisorption appears not to be reversible and leads to a more negative surface charge.[16] Furthermore, the zeta potential of $CaCO_3$ at 25 °C is more negative than at 55 °C with the same concentration of K-oleate. This indicates that more oleate ions take part in the ion exchange reaction on the $CaCO_3$ particle surface at lower temperature.

Addition of the polymer NaPAA causes the zeta potential to initially decrease sharply, reaching an almost constant value (around −70 mV at 25 °C and −75 mV at 55 °C) at higher NaPAA concentrations (Figure 1b). The initial decrease in the zeta potential with polymer concentration is clearly attributed to the effect of NaPAA adsorption, which is expected to be a fast process. The constant zeta potential for polymer concentrations of 50 ppm and above suggests that the particle surface is saturated with a layer of polymer. The zeta potential value at 55 °C is lower than that at 25 °C, indicating that more PAA^- ions adsorbed on the particle surfaces at higher temperature.

The adsorption of polymer and the surfactant influences the formation and growth of the $CaCO_3$ particles, as identified by DLS measurements (Figure 4). Here, it should be noted that after sedimentation only the small and colloidally stable particles in the supernatant contribute to the scattering. The DLS data also show that particles in the supernatant are finely dispersed with a rather narrow size distribution and particle sizes of only a few hundred nanometers.

For K-oleate, the size of the $CaCO_3$ particles initially decreases sharply with concentration up to 50 ppm followed by a gradual increase in size when the concentration is further increased (Figure 4b). This reflects the fact that adsorption has two opposite effects on the particle size; namely, it can inhibit particle growth and it can also increase the particle size either by forming a thick surface layer or by aggregating particles. When the K-oleate was present in the solution at low concentration, the adsorption of oleate ions on the surface of $CaCO_3$ particles inhibited the formation and growth of crystal. Hence, the particle size decreases sharply with increasing oleate concentration. At the same time, the amount of K-oleate adsorbed on the particle surface will increase with the concentration of K-oleate. The larger amount of oleate on the particle surface is also reflected in the sharp decrease of the surface potential. At sufficient high oleate concentration, this leads to precipitation of calcium dioleate, which in turn gives rise to an increase of particle size as discussed above. The process at 55 °C is more distinct than for 25 °C, and consequently, the surface potential is more negative at 55 °C than at 25 °C. Another factor, which will be discussed further below, is that the crystal structure changes with temperature. Such changes can also affect the adsorption/deposition of the oleate on the surface of the particles and hence both size and charge of the particles.

Figure 4b shows the corresponding results for the addition of NaPAA. In this case, the particle size also shows sharp initial decreases with concentration of NaPAA, but this is followed by a constant size with further increase of NaPAA concentration. This indicates that the presence of NaPAA completely inhibits the growth of $CaCO_3$ particles in the solution. In addition, the particle size at 55 °C is generally smaller than that at 25 °C. This indicates a stronger binding of NaPAA to $CaCO_3$ at the higher temperature, which in turn inhibits the growth of the particles. The nanometer-sized particle stabilized with the polymer will remain dispersed in the solution for a considerable time without sedimentation. From the results above, we conclude that the polymer NaPAA is more efficient in

DOI: 10.1021/acsami.5b04679
ACS Appl. Mater. Interfaces 2015, 7, 21115−21129

inhibiting the formation and growth of $CaCO_3$ particles compared to the soap.

3.3. Crystal Structure and Morphology of Large $CaCO_3$ Particles Formed in the Bulk Solution. The morphology and structure of $CaCO_3$ crystal formed at 55 °C in the presence of different concentrations of K-oleate in bulk solution and collected from the sediment are shown in Figure 5.

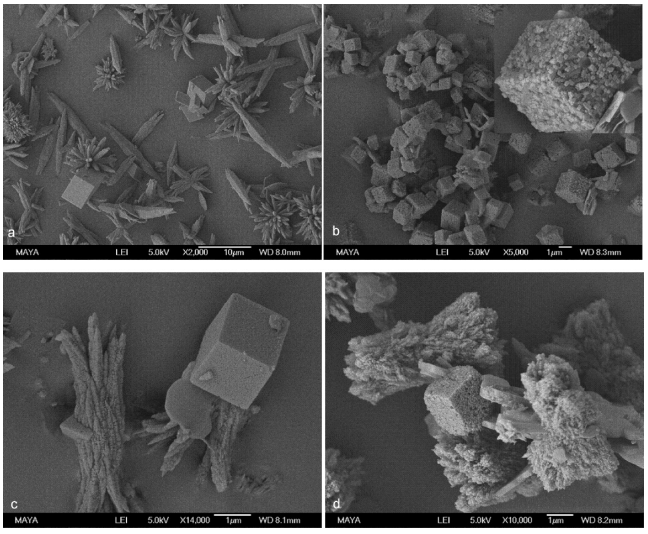

Figure 5. SEM images of $CaCO_3$ crystal formed in the bulk solution with different concentrations of oleate at T = 55 °C and pH 10: (a) 0; (b) 50 ppm; (c) 200 ppm; (d) 400 ppm. The reaction time is 1 h.

Without K-oleate in the solution (Figure 5a), $CaCO_3$ crystals form two types of crystals, namely, aragonite and calcite. The morphology of calcite crystals is that of a distorted cube, and aragonite crystals are needle- or flowerlike. However, when the K-oleate concentration is 50 ppm in the solution (Figure 5b), the rhombohedral calcite dominants in the samples, and there are some plate-like Ca-soap aggregates. Furthermore, in the presence K-oleate, the surface structure of the formed crystalline superstructures increased in roughness and there are many tiny cubic crystals adsorbed on the surface of calcite crystal (Figure 5b). All of the described crystal morphologies appear to be very stable, once they are formed. The flower-like aragonite crystal dominates when the concentration of K-oleate is 200 ppm (Figure 5c), and there is also more irregular Ca-soap aggregation formed in the samples. On the basis of the low solubility product of 2.51×10^{-12} for calcium oleate at 67 °C and pH 9,[48] this increase of irregular aggregates is most likely connected to the precipitation of calcium oleate. It is clear that K-oleate addition changes the crystal shapes from low axial ratio forms such as cubes (calcite) to higher axial ratio rods (aragonite). The latter type of crystallites becomes more elongated in shape as the soap concentration increases. The presence of fatty acid soaps like oleate have been shown to influence all three key steps of $CaCO_3$ precipitation: nucleation, crystallite growth, and aggregation.[49] Furthermore, the presence of oleate can be used to prepare hydrophobic $CaCO_3$ nanoparticles.[49,50] As the concentration of K-oleate increases to 400 ppm (Figure 5d), more Ca-oleate precipitations cover the crystal surfaces and more irregular aggregates appear in the sample.

The corresponding SEM images of $CaCO_3$ crystals formed from hard water with K-oleate at 25 °C are shown in Figure 6.

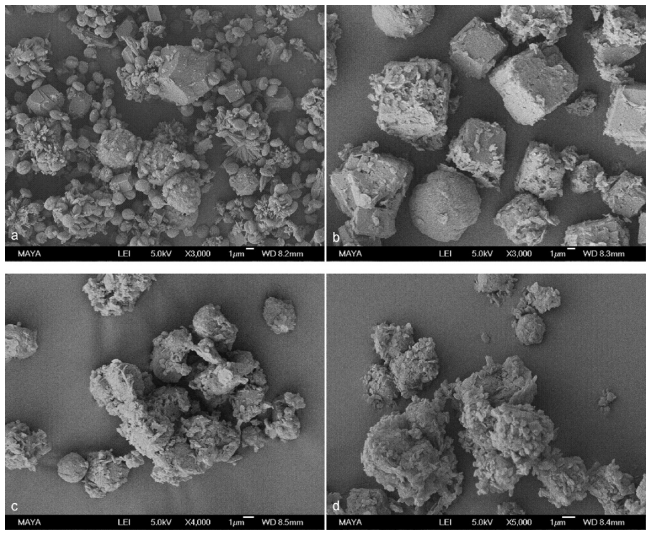

Figure 6. SEM images of $CaCO_3$ crystal formed in the bulk solution with different concentrations of oleate at T = 25 °C and pH 10: (a) 0; (b) 50 ppm; (c) 200 ppm; (d) 400 ppm. The reaction time is 1 h.

The images show that larger particles are formed at the higher concentration of oleate (Figure 6). This is consistent with the higher turbidity (Figure 1) that reflects the more pronounced and extensive aggregation process at higher oleate concentration. All three crystalline polymorphs and amorphous particles are observed when there is no K-oleate in the solution (Figure 6a). The amorphous particles as well as the vaterite particles progressively disrupt into small particles during the course of the polymorphic transformation.[51] Calcite crystals grow larger and their surface becomes rougher. At a K-oleate concentration of 50 ppm (Figure 6b), the rhombohedral calcite crystals are predominant in the samples, but there are also quite a few spherical particles. The surface of these particles is pretty rough because of the coprecipitation with Ca-oleate. As the concentration of K-oleate increases (Figure 6c,d), there are more Ca-oleate covered crystals and aggregates in the sample, while the type of crystal structure in the sample does not seem to change.

The XRD results shown in Figure 7 verify the crystal structures based on the morphology of the crystals. The samples prepared at 55 °C (Figure 7a) are quite different from those prepared at 25 °C as expected from the SEM images. For the 55 °C samples, the calcite structure dominates with 50 ppm K-oleate. However, when increasing the K-oleate to 200 ppm aragonite and vaterite, crystals appear and a further increase of K-oleate concentration appears not to change the ratio between aragonite or vaterite and calcite. The decrease in intensity of the XRD diffractogram can be interpreted as a loss of crystalline structure. The XRD pattern for the 25 °C samples shows the sharp peaks of calcite, and there is no significant amount of other type of crystals in the sample (Figure 7b). However, the spherical particles observed in the SEM images are likely to be amorphous $CaCO_3$ as no diffraction pattern could be detected from them. The amount of calcite sharply decreased with the increase of K-oleate soap from 50 to 200 ppm, which indicates that the formation and growth of $CaCO_3$ particles were inhibited gradually with an increase of K-oleate concentration. We can conclude that the polymorph of crystalline $CaCO_3$ depends on the additive and temperature in the solution. At low temperature, the amount of metastable polymorphs,

DOI: 10.1021/acsami.5b04679
ACS Appl. Mater. Interfaces 2015, 7, 21115−21129

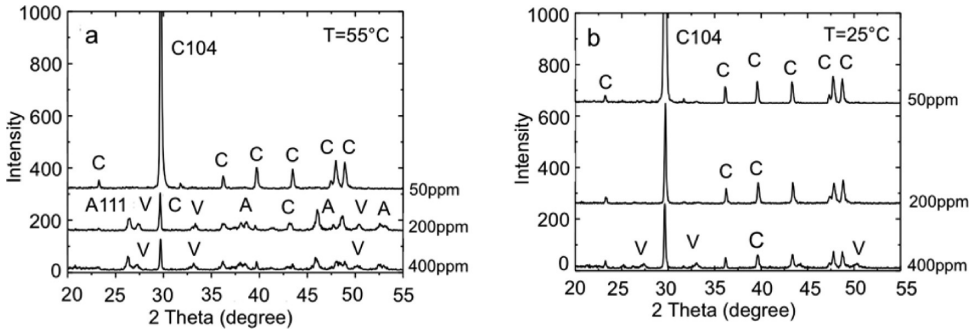

Figure 7. XRD patterns of $CaCO_3$ crystals formed in the presence of K-oleate obtained at 55 °C (a) and 25 °C (b), and pH 10. "A", "C", and "V" denote peaks from aragonite, calcite, and vaterite, respectively.

aragonite and vaterite, is reduced by the presence of oleate. The most thermodynamically stable polymorphic form, calcite, therefore prevails in the sample.

SEM images of $CaCO_3$ formed in the bulk with NaPAA concentration at 25 and 55 °C are shown in Figure. 8. The

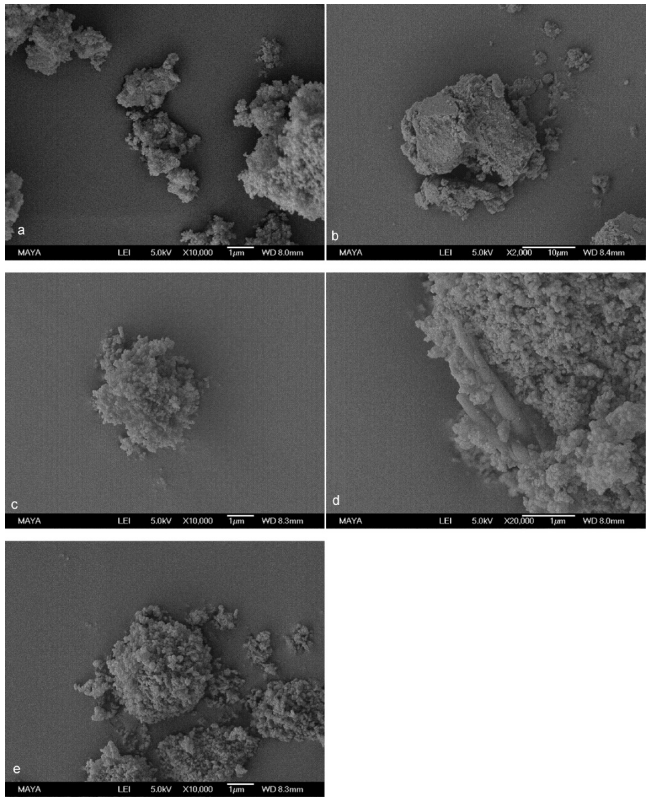

Figure 8. SEM images of $CaCO_3$ precipitates formed from hard water with NaPAA at different temperatures. T = 25 °C: (a) 50 ppm, (b) 200 ppm; T = 55 °C: (c) 50 ppm, (d) 200 ppm, and (e) 400 ppm. The reaction time is 1 h and pH is 10.

morphology of $CaCO_3$ particles in bulk solution with NaPAA at 25 °C was drastically changed (Figure 8a) compared with those observed in the absence of NaPAA (Figure 6a). Here, (amorphous) nanosized particles were formed instead of crystals, and these small particles are found to aggregate into large particles when the dispersion is centrifuged. This seems not be very much affected by the polymer concentration as the images recorded at 200 ppm polymer (Figure 8b) are similar to those recorded for 50 ppm. However, we note that the amount of tiny particle decreases, the number of large aggregates increase, and they appear to be denser. The XRD patterns (not shown) do not show any crystallinity in the samples, which indicates that they mainly contain amorphous $CaCO_3$ and Ca-soap aggregates.

The images recorded at 55 °C are quite similar to those obtained at 25 °C except for 200 ppm polymer (Figure 8d), which shows larger aggregates. When the polymer concentration is 50 ppm, the nanosized particles also formed and aggregated into large particles. It is very difficult to identify the structure and type of these particles based only on the SEM images. The corresponding XRD pattern showed that there are three kinds of crystal in the sample, aragonite, calcite, and vaterite. The aragonite crystal dominates in the samples, and the content of calcite and vaterite is fairly low (Figure 9). The

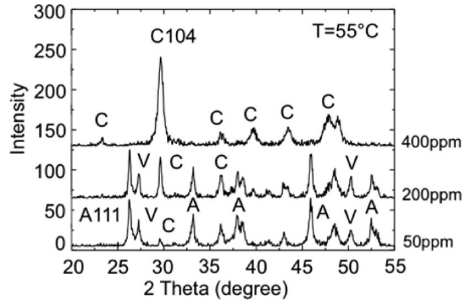

Figure 9. XRD patterns of $CaCO_3$ precipitate with NaPAA obtained at pH 10 and 55 °C. "A", "C", and "V" denote peaks from aragonite, calcite, and vaterite, respectively.

occurrence of vaterite in the presence of poly(acrylic acid) was also observed by Naka et al.,[25] who found that vaterite is stabilized by this polymer. Nanosized particles for 200 ppm of NaPAA in addition to a few needle-like crystals formed in the sample, which is typical for aragonite crystals (Figure 8d). The XRD results show that the amount of aragonite is almost the same as at the lower polymer concentration, while the content of calcite increases significantly. The SEM images of sample with 400 ppm polymer are very similar to those recorded at 50 ppm (Figure 8e). However, the XRD diffractogram is clearly different from those for 50 and 200 ppm polymer. The calcite is dominant in the sample, and aragonite disappears totally. It also is important to note that the XRD intensity for all three samples is significantly lower, suggesting that crystallinity in the sample is very low. This is attributed to the fact that the anionic groups of NaPAA can bind a sufficient amount of Ca^{2+} ions to inhibit the association of Ca^{2+} and CO_3^{2-}, which in turn can

DOI: 10.1021/acsami.5b04679
ACS Appl. Mater. Interfaces 2015, 7, 21115−21129

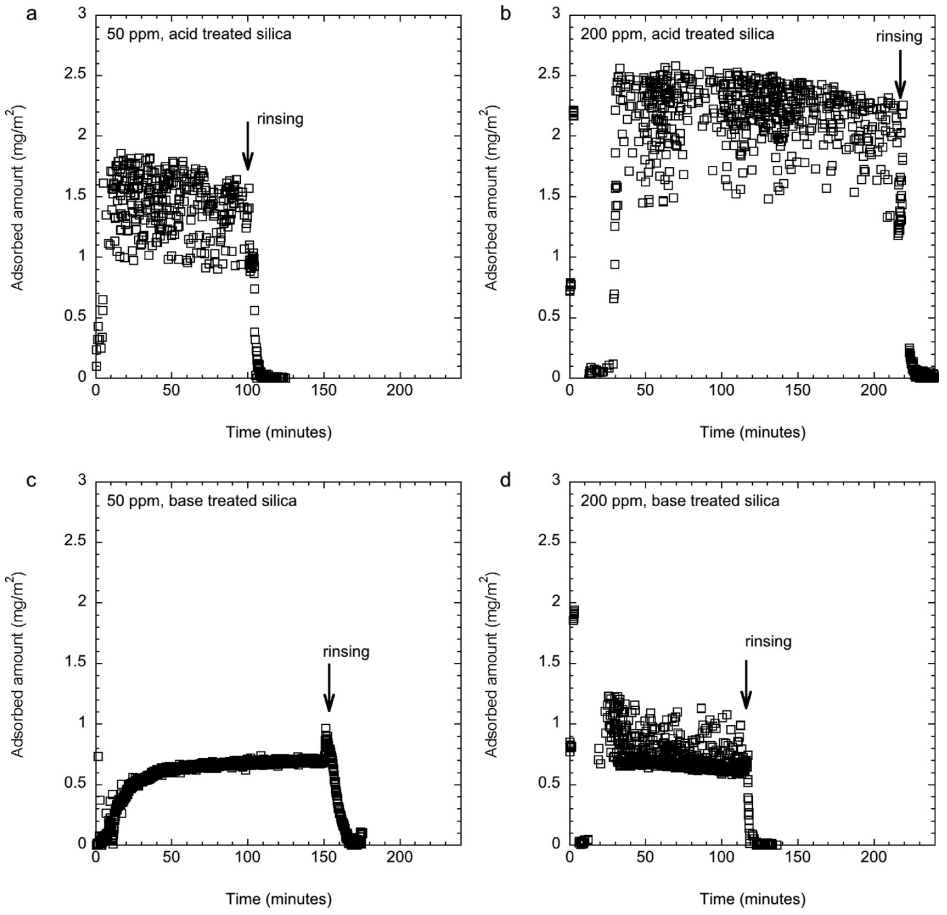

Figure 10. Adsorbed amount from a dispersion of $CaCO_3$ particles with different concentrations of NaPAA (50 and 200 ppm) on the acid (a and b) and base (c and d) treated silica surfaces at T = 25 °C and pH 10.

prevent the precipitation of calcium carbonate. The polymer can thereby affect different steps of the crystallization process of $CaCO_3$ including forming a complex with ions, nucleation, stabilizing intermediate amorphous particles, and controlling the assembly of so-called mesocrystals.[19] The polymer NaPAA can therefore inhibit the formation and growth of $CaCO_3$ particles as they adsorb on the $CaCO_3$ crystal surface.

3.4. Kinetics of $CaCO_3$ Deposit Formation on Solid Surfaces. Ellipsometry was used to follow the kinetics of the crystal deposition/formation on hard surfaces in the presence of polyelectrolyte as NaPAA turned out to be the most promising with respect of reducing crystal growth. In addition, the solution turbidity in the presence of oleate was too high to use ellipsometry to in situ follow the deposition process. The studies were conducted under conditions that mimic the ADW conditions, namely, at pH 10 and with hard water (21°dH, 4 mM Ca^{2+}) using different concentrations of polyelectrolyte. The surface deposition was monitored and correlated to the formation and growth of $CaCO_3$ particles in bulk and at surfaces. Figure 10 shows the adsorbed amount from a $CaCO_3$ dispersion in the presence of NaPAA on an acid treated silica surface (Figure 10a,b) and base treated silica surface (Figure 10c,d) at 50 ppm (Figure 10a,c) and 200 ppm (Figure 5b,d). The adsorbed amount on all surfaces increased sharply with time when polymer NaPAA was added to the hard water until it reached a plateau value. For the acid treated silica surface, the adsorbed amount of polymer or particle increases with increasing polymer concentration. For the base treated silica surface, however, the adsorbed amount is not significantly affected by the polymer concentration. We also note that the adsorbed amount at the acid treated silica surface is 2 to 3 times larger than that at the alkali treated silica surface. In order to test the reversibility of the deposition, the bulk solution was continuously replaced with water (rinsing step using 20 times the volume of the cuvette). The results show that, when rinsing with pure water was performed (arrow shown in Figure 5), total desorption occurred within minutes, suggesting that the deposited layer is reversibly attached to the silica surface. The adsorption mechanism can be thought of as either adsorption of polymer film on the surface or attachment of crystals to the surface. The initial increase of adsorbed amount is likely due to the adsorption of polymer on the hard surface. On the basis of the experimental data, the adsorption process in the presence of $CaCO_3$ can be divided in two steps. First, the added polymer molecules adsorb on the hard surfaces as well as on particle surfaces in the dispersion, respectively. Then, the particles covered with polymer adsorb on the hard surface with adsorbed polymer. The adsorption of polymer on the substrate can also inhibit the particle deposition. As reported previously, polymers and other scale control additives affect $CaCO_3$ crystallization in a multitude of ways. This includes molecular binding of Ca^{2+} ions, affecting nucleation and growth of crystals, as well as stabilizing the formed crystals as dispersant against aggregation.[31]

3.5. $CaCO_3$ Crystal Morphology of Hard Surfaces. The solid surface is not expected to affect the crystallization

DOI: 10.1021/acsami.5b04679
ACS Appl. Mater. Interfaces 2015, 7, 21115−21129

pathway, but the crystallization process affects the surface deposition and which particles can attach to the surface. Here, the surface properties of the substrate play a crucial role in determining which types of calcium carbonate particles are adsorbed/formed at a solid surface.[51,52] In order to be able to relate precipitation to the particle adsorption, it is important to characterize the calcium carbonate particle size and shape both formed in the bulk and on the substrates. The $CaCO_3$ crystal morphology and structure on different hard surfaces in the presence of K-oleate and NaPAA at 55 and 25 °C were studied by SEM. Representative SEM images of $CaCO_3$ crystals formed/deposited on stainless steel and acid treated silica surfaces, recorded after 1 h at 55 °C, are shown in Figure 11.

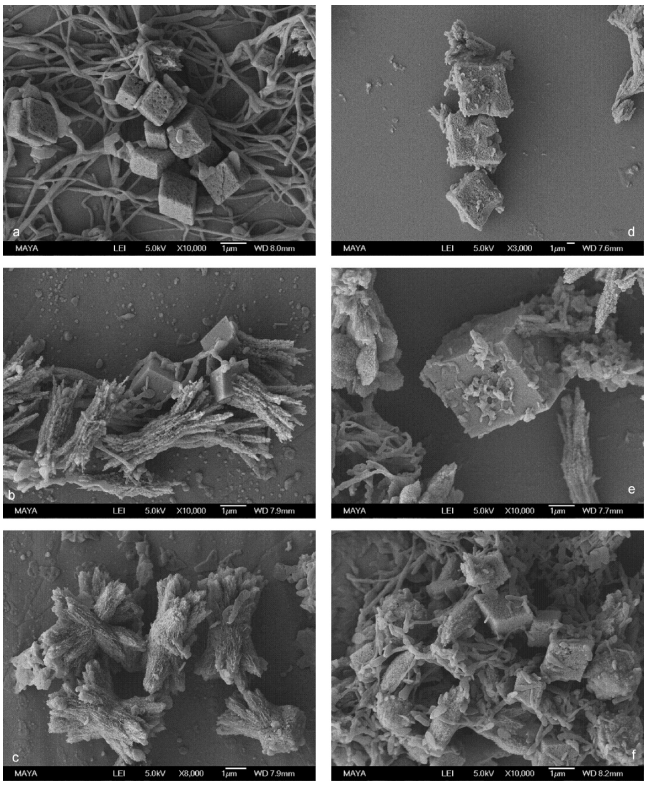

Figure 11. SEM images of $CaCO_3$ crystals formed in the presence of K-oleate at different concentrations on hard surfaces at T = 55 °C and pH 10. (1) Stainless steel surface: (a) 50 ppm, (b) 200 ppm, and (c) 400 ppm. (2) Acid treated silica surface: (d) 50 ppm, (e) 200 ppm, and (f) 400 ppm. The reaction time is 1 h.

Here, it should be noted that the $CaCO_3$ crystals on the base treated silica surface were almost identical to those on the acid treated silica surface and are therefore not shown. Also, on the surface, two types of $CaCO_3$ crystals, namely, calcite and aragonite, dominate (Figure 11). In contrast to the crystals formed in bulk dispersion (Figure 5b), the rhombohedral calcite crystal is predominant on hard surfaces in addition to a few flowerlike aragonite crystals that were observed in the presence of 50 ppm K-oleate (Figure 11a,d). This indicates that the calcite crystals are more likely to adhere/form on the surface than the other polymorphs. However, at high concentration of K-oleate, the flowerlike aragonite crystal is predominant on the surfaces (Figure 11c,f). The fibril-like aggregates in Figure 11a are most likely Ca-soap aggregates. The surface morphology of crystals becomes rather rough and porous. In addition, more amorphous particles and Ca-soap aggregates adsorbed on the surface of crystals are observed with increasing K-oleate concentration. The size of the crystals on the surface are about 3 μm for calcite and 5 μm for aragonite, which is almost the same size as those formed in the bulk solution. This suggests that these crystals are formed in bulk and then attach to the surface. It should be noted that, when the substrate is acid treated silica (Figure 11d–f), the amount of crystals on the surface is significantly lower compared with the amount of crystals on the stainless steel surface. The observed difference in adsorbed amount can be attributed to the surface properties. When the pH value of an aqueous solution is above pH 7, the surface charge of silica and stainless steel should be negative.[35,37,38,53,54] Though the surface charge for stainless steel in the solution is rather similar to the acid treated silica surface, the stainless steel surface is considerably rougher than the silica surface. This might provide more defects that can act as sites for adsorption of crystals on the surface. The adsorbed amount of $CaCO_3$ particles on the stainless steel surface is consistently larger than those on the silica surfaces.[51]

The corresponding SEM images of $CaCO_3$ crystal formed in the presence of K-oleate on hard surfaces at 25 °C are shown in Figure 12. Similar to the particles in bulk solution, the calcite

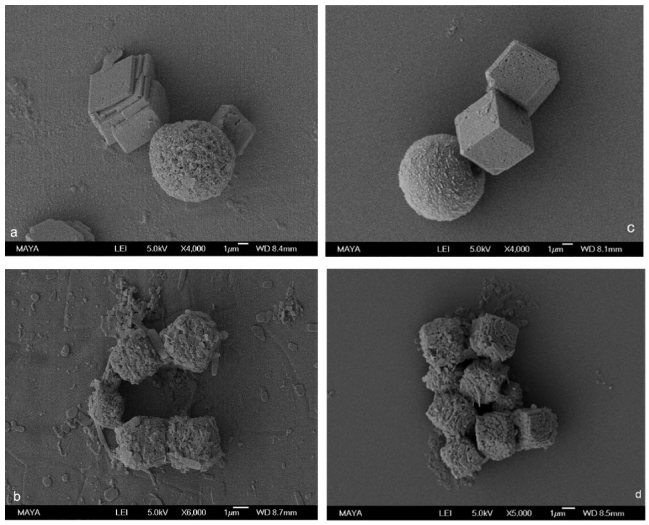

Figure 12. SEM images of $CaCO_3$ crystals with K-oleate concentration on hard surfaces at T = 25 °C and pH 10. (1) Stainless steel surface: (a) 50 ppm and (b) 200 ppm. (2) Acid treated silica surface: (c) 50 ppm and (d) 200 ppm. The reaction time is 1 h.

crystal is predominant in all the samples. Two types of $CaCO_3$ particles formed in the presence of 50 ppm K-oleate adsorb/form on both types of hard surfaces, namely, rhombohedral calcite crystal and spherical particles with a size of 5 μm (Figure 12a,c). On the stainless steel surface, the calcite crystal is staircase-like and the spherical particles are looser and pretty rough. In contrast, the calcite appears as regular cubic crystals and the spherical particle is denser and smoother on the acid treated silica surface. The amount of irregular Ca-soap aggregates on both surfaces increases with the concentration of soap, and the surface of crystal particles and substrates becomes rougher.

The time dependence of the $CaCO_3$ deposition on stainless steel, acid treated silica, and base treated silica incubated in hard water with NaPAA was followed for 10 min, 1 h, and 10 h at 25 and 55 °C. However, we did not observe any $CaCO_3$ crystal adsorbed on the surfaces when the incubation time is 10 min

DOI: 10.1021/acsami.5b04679
ACS Appl. Mater. Interfaces 2015, 7, 21115–21129

for both temperatures and 1 h for 55 °C. Thus, only SEM images of samples obtained after 1 h at 25 °C and 10 h at 55 °C will be discussed. The adsorbed amount of particles at 25 °C is fairly low in all samples, and only a few irregular small particles are found on the surfaces (Figure 13a). In fact, particles were

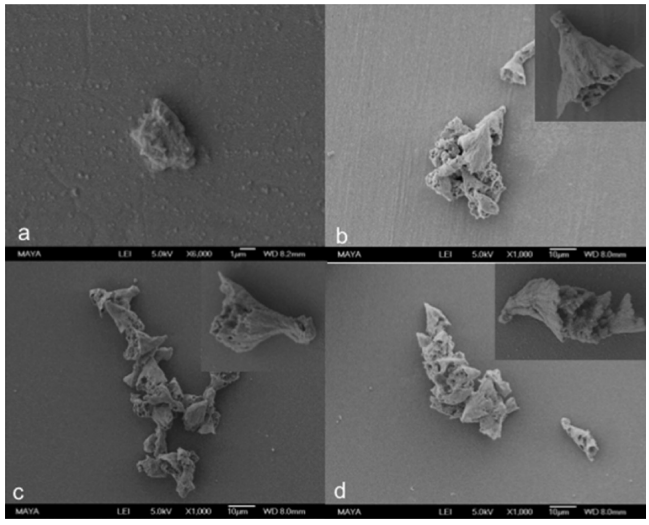

Figure 13. SEM images of $CaCO_3$ crystals with NaPAA concentration (200 ppm) on hard surfaces at 25 °C and 1 h for (a) and 55 °C and 10 h for (b–d). (1) Stainless steel surface: (a and b). (2) Acid treated silica surface: (c). (3) Base treated silica surface: (d).

only observed on the stainless steel surface at 25 °C. The substrate surfaces became rougher because of the adhesion of polymer film on the surface. The adsorbed amount and thickness of polymer layer on the surface should be around 2.5 mg/m^2 by ellipsometry measurements (Figure 10) and 80 nm thick as estimated from the AFM measurements (Figure 14). In addition, the amount of particle on the stainless steel surface is larger than on the two silica surfaces, which can be attributed to the rougher surface of stainless steel. The SEM images in Figure

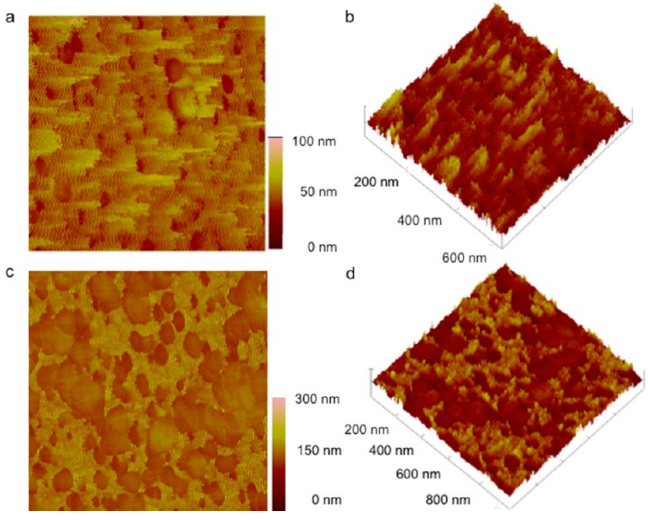

Figure 14. Taping-mode AFM height images (a and c) and the corresponding 3D images (b and d) of adsorbed layer on the acid treated silica surface from hard water with different concentrations of NaPAA for 1 h: (a and b) 50 ppm, (c and d) 200 ppm. T = 25 °C and pH = 10.

13b–d show that there is no large difference between $CaCO_3$ deposits on three surfaces at 55 °C. There is only one kind of crystal adsorbed on the surface, and the adsorbed amount is fairly low. They seem to be trumpet-like aragonite crystals, and these particles tend to aggregate on the surface. From Figure 13, it appears that the particles adsorbed on the surfaces were also well covered by NaPAA. It is clear that the presence of polymer NaPAA inhibits the crystallization of $CaCO_3$ in bulk and significantly reduces $CaCO_3$ particle deposition/formation on the different surfaces. This is likely due to the effect of polymer adsorbing to the growing crystal as well as to the hard surfaces.

AFM measurements were performed to gain insight into the morphology and structure of $CaCO_3$ in the presence of polymer on a hard silica surface on the nanometer scale. Figure 14 presents typical images of layers formed on the silica surface from $CaCO_3$ solution with NaPAA after 1 h. The images feature a layer with high roughness and islands of rather well-defined crystals. This indicates that the layer closest to the hard surface consists of NaPAA. At 50 ppm (Figure 14a,b), both continuous domains and islands are observed and the surface is pretty rough. The height of this film is about 40 nm. We note that there is a streaky pattern at low polymer concentration. This can possibly be a consequence of material being moved around on the surface by the tip. Randomly distributed patches with a thickness of about 80 nm are observed when the concentration of polymer reaches to 200 ppm (Figure 14c,d). In addition, the surface at 200 ppm appears to be smoother than that at 50 ppm. The observed increase of the surface layer thickness with polymer concentration means that the polymer either adsorbed as aggregates or adopted a more extended conformation and protruded into the solution. These results are in good agreement with ellipsometry results on the acid treated silica surface.

4. DISCUSSION

4.1. Formation and Growth Mechanism of $CaCO_3$ Crystals with Polyelectrolyte and Soaps in the Bulk.

The classical nucleation theory of $CaCO_3$ as well as from the recently presented findings of a prenucleation cluster pathway[1,5] give important leads that can explain the formation and growth mechanism of $CaCO_3$ in the studied system. The addition of an interacting polymer, NaPAA, or surfactant, oleate, to the crystallization solution can modify the ongoing processes in various different ways:[26]

(1) The polymer or surfactant can block or retard the clustering of single ions to the nucleus by forming a complex with the ions, which makes assembly effects more significant than the classical crystallization route. This is particularly important for the oleate, which is known to form dicarboxylic acids bridged by calcium ions.[18,20] This can in turn lead to formation of larger aggregates.

(2) The additive can act as a nucleation agent by lowering the interface energy of subcritical and critical nuclei, increasing the number of primary nanoparticles.

(3) Metastable intermediates stabilized by colloidal forces, such as amorphous precursor structures, can be formed and prevent/retard crystallization.

(4) The shape/properties of the primary nanoparticles can be changed by selective adsorption and/or enrichment

DOI: 10.1021/acsami.5b04679
ACS Appl. Mater. Interfaces 2015, 7, 21115–21129

onto specific crystal faces, which inhibits growth from these crystal faces.

First, we would like to point out that not only one mechanism can explain our results, but one should consider a competition of the different processes, 1−4. The type of additive and the concentration of the additive determine the relative importance of one mechanism compared to the other. We observed clear effects of the type of additive on the surface structure and morphology of the formed $CaCO_3$ crystals.

The addition of minor amounts (50 ppm) of soap (K-oleate) had two effects. On the one hand, all the crystalline species became very homogeneous in morphology and size. This is easily explained by a better control of nucleation by the surfactant, which is also reflected by the increasing number and decreasing size of $CaCO_3$ particles with increasing oleate concentration as shown by the DLS and turbidity results. The observed tiny (cubic) crystals on the surface of calcite crystal in the presence of oleate indicate that the crystallization mechanism changes from ionic growth to mesoscale assemble according to route (1). The formed crystalline superstructures become rougher, and some crystal corners/edges became rounded (Figure 5b).

The presence of polymer, NaPAA, on the other hand, leads to the formation of nanosized particles that appear to aggregate into large particles after centrifuging the dispersion. A polymer NaPAA can alter the shape of the primary nanoparticles by selective adsorption and/or enrichment onto specific crystal faces, which leads to growth inhibition of these crystal faces. The route (4) could therefore explain the mechanism of $CaCO_3$ crystallization in the presence of NaPAA. Thus, this type of polymer has the potential to control or even inhibit the growth of crystals in the bulk solution. Likewise, additives such as polyelectrolytes were shown to be capable of stabilizing nanosized $CaCO_3$ particles,[2,55] because they can effectively increase their colloidal stability.[34,56] In fact, we observed from the DLS and turbidity data that the $CaCO_3$ particles formed in the presence of the polyelectrolyte were smaller and also more stable against sedimentation than those formed in the presence of K-oleate. Furthermore, as a polyelectrolyte, NaPAA, strongly binds free Ca^{2+} ions, and the free Ca^{2+} ion concentration decreases and thus slows down the related speed of crystal growth.[57] When the relative amount of carbonate ions increases, they will compete with the PAA ions for the highly localized and enriched Ca^{2+} close to the NaPAA backbone, presumably initially forming a mixed nanoparticle composed of hydrated, amorphous $CaCO_3$ and NaPAA.

4.2. Adsorption Mechanism of $CaCO_3$ Particles on Hard Surfaces in the Presence of Polyelectrolyte and Surfactant. It is clear that the presence of oleate and NaPAA results in drastic changes in the crystallization of $CaCO_3$ as well as the colloidal stability of the formed particles. This leads to significant reduction in the tendency of $CaCO_3$ to adsorb on the different surfaces. The attachment of $CaCO_3$ particles to hard surfaces is at least partly controlled by the surface charge and the structure of the surfaces. Here, it should be noted that silicon surfaces always have a spontaneously formed oxide layer that, when exposed to water, contains surface silanol groups. Silanol groups are amphoteric: they can act as either a donor or acceptor of a proton. The average charge density of silanol groups on the silica surface varies with the pH and added salt.[35,54] When the pH value of an aqueous solution is above pH 2.5, the net surface charge of silica is expected to be negative. The alkali treated silica surface has more negative surface charge density compared to an acid treated silica in alkali solution.[53] The surface charge for stainless steel (304) is also pH dependent. The zero net charge (IEP) for stainless steel particles is attained at pH ∼ 3.4, and similar values were obtained for a flat stainless steel surface with streaming potential measurements; i.e., the surface has a negative charge at alkaline pH values.[37,38] Cationic polyelectrolytes readily adsorb to the silica surface because of the attractive interaction with the oppositely charged surface.[54,58−60] This is not the case for anionic polyelectrolyte, where the electrostatic repulsion between the polymer and the ionized silanol groups prevents adsorption. However, the presence of Ca^{2+} ions will efficiently screen the electrostatic repulsion between the anionic polyelectrolyte and the negative silica surface. In addition, they can bind strongly to the anionic polyelectrolyte and even reverse the effective charge of the polymer and also in the case of neutralization decrease the solubility of the polymer. Both factors will promote polymer adsorption. Furthermore, Ca^{2+} is shown to interact strongly with the silica surface to reduce and even reverse the charge.[61] This is indicated in Figure 15. In addition, the silica surface has a fairly low negative surface charge density even at alkaline pH, typically about, 320 Å^2 per charge for silica, depending on the ionic strength.[54] In addition, the silica surface is expected to have some siloxane groups which are more hydrophobic,[35] and therefore, the hydrophobic chain of polymer can interact with these surface groups, promoting polymer adsorption. In fact, strong hydrophobic interactions may overcome the loss of entropy and electrostatic repulsion, and therefore, even anionic polyelectrolytes under the conditions used in the present study can adsorb to the surface.[59,60] The adsorbed amount of the anionic polymer is higher on the acid treated silica surface than on the base treated silica surface, which has a higher negative charge density

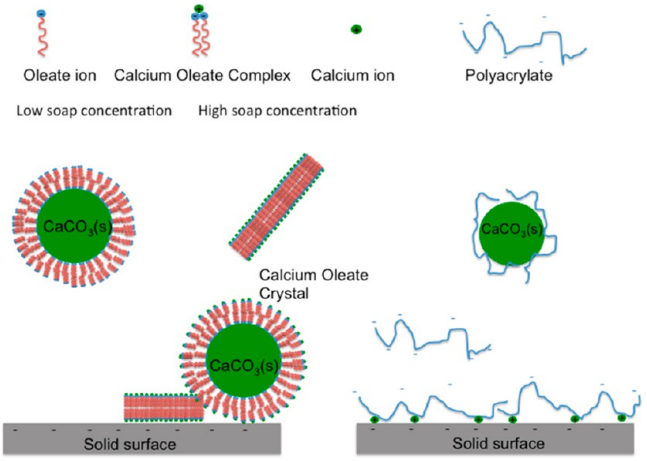

Figure 15. Schematic representation of how oleate and polyelectrolyte (polyacrylate) can reduce deposition of $CaCO_3$ on surfaces, by preventing particle growth and passivation of the surface. Two cases are shown for oleate: low soap concentration with low deposition and high soap concentration with codeposition of soap and $CaCO_3$. Note that smaller particles are formed in the presence of the polymer and that separate calcium oleate crystals are likely to form in the presence of oleate and calcium. For both, the anionic polymer and oleate binding of calcium facilitates adsorption on the negatively charged surface. In the case of oleate, each calcium binds two fatty acids according to Scheme 1a−1c.

DOI: 10.1021/acsami.5b04679
ACS Appl. Mater. Interfaces 2015, 7, 21115−21129

(Figure 10).[42] The adsorbed amount on the stainless steel surface is close to that on the acid treated silica surface. Here, it should be noted that the stainless steel surface is considerably rougher than the silica surface and might therefore provide a larger effective surface area as well as more defects for adsorption of polyelectrolyte and the particles on the surface.

It should also be noted that the oleate also potentially makes the crystals more hydrophobic, which is used in flotation applications.[16] This effect can explain the larger particles due to aggregation and subsequent sedimentation in the case of oleate.

5. CONCLUSION

The aim of this study was to provide the necessary knowledge to develop processes and additives that reduce calcium carbonate deposition during the ADW process. We have investigated the effect of K-oleate and NaPAA on the crystallization behavior of $CaCO_3$ in the bulk solution and on hard surfaces at different temperatures and found that the surfactant or polymer plays a critical role in controlling the nucleation and growth of $CaCO_3$ crystal as well as their adsorption on hard surfaces. On the basis of the results obtained from SEM, ellipsometry, and DLS measurements, it is clear that the presence of additives, especially polymer NaPAA, hampers the $CaCO_3$ crystallization and crystal growth in bulk. These formed particles were also found to have higher colloidal stability. The polymer was therefore found to significantly reduce $CaCO_3$ particle deposition/formation on the different surfaces.

The inhibition of $CaCO_3$ particle adhesion can be attributed to the adsorption of the polymer on the growing crystal and on the solid surfaces. The presence of the inhibitor also changes the crystal morphology of both the adhered and precipitated crystals, which in turn hampers crystal growth.[31] Figure 15 schematically illustrates a situation where the additives inhibit deposition by adsorbing both to the substrate and particle surface. The electrostatic repulsion between adsorbed surfactant or polymer and coated $CaCO_3$ particles in the bulk is thought to be one of the main factors that limits the particle deposition. In the case of the polymer, steric repulsion is likely to contribute. The formed particles in the presence of the polymer were also found to have higher colloidal stability. The polymer was therefore found to significantly reduce $CaCO_3$ particle deposition/formation on the different surfaces. Here, also polymer adsorption on the hard surfaces would contribute.

The influence of the fatty acid soap, K-oleate, is more complex. At low concentration, the K-oleate seems to reduce crystal growth by adsorption to the $CaCO_3$ particle surface. This is consistent with the efficiency of soaps where, e.g., potassium oleate is one of the common surface-active components used in industrial applications like flotation. Our experimental results indicate that calcium oleate crystals are likely to form in the presence of oleate and calcium. Such crystals or aggregates can also adhere to the solid surface as well as to the $CaCO_3$ crystals. There will always be a competition between the adsorption on the already formed $CaCO_3$ crystals and the formation of separate calcium soap aggregates that eventually can attach to already formed $CaCO_3$ crystals or provide the nucleation site for $CaCO_3$ crystal growth. In order to be able to separate between the two mechanisms, more extensive kinetic studies are required beyond the scope of the present study. At high K-oleate concentration, the formation of codeposits of calcium soaps and $CaCO_3$ is apparent both in bulk and at the interface. The formation of such codeposits is partly due to hydrophobic interaction. In the ADW application, the high soap concentration corresponds to the cleaning of greasy dishes.

The present study shows that, in order to understand the mechanism of surface deposition of $CaCO_3$ on solid surfaces in order to control it by additives, one needs to consider the bulk crystallization as well as the colloidal stability of the formed particles. It is clear that the polymer NaPAA is much more efficient than the K-oleate in inhibiting the deposition of $CaCO_3$ on hard surfaces in the ADW (automatic dishwasher) process. This is manifested by the significantly smaller and more stable $CaCO_3$ particles against sedimentation and deposition.

AUTHOR INFORMATION

Corresponding Author

*E-mail: Tommy.Nylander@fkem1.lu.se.

Notes

The authors declare no competing financial interest.

REFERENCES

(1) Gebauer, D.; Kellermeier, M.; Gale, J. D.; Bergström, L.; Cölfen, H. Pre-Nucleation Clusters as Solute Precursors in Crystallisation. *Chem. Soc. Rev.* **2014**, *43*, 2348−2371.

(2) Gower, L. B. Biomimetic Model Systems for Investigating the Amorphous Precursor Pathway and Its Role in Biomineralization. *Chem. Rev. (Washington, DC, U. S.)* **2008**, *108*, 4551−4627.

(3) Dickinson, S. R.; McGrath, K. M. Aqueous Precipitation of Calcium Carbonate Modified by Hydroxyl-Containing Compounds. *Cryst. Growth Des.* **2004**, *4*, 1411−1418.

(4) Gaines, R. V.; Skinner, H. C. W.; Foord, E. E.; Mason, B.; Rosenzweig, A. *Dana's New Mineralogy*, 8th ed.; Wiley: New York, 1997.

(5) Gebauer, D.; Völkel, A.; Cölfen, H. Stable Prenucleation Calcium Carbonate Clusters. *Science* **2008**, *322*, 1819−1822.

(6) Addadi, L.; Raz, S.; Weiner, S. Taking Advantage of Disorder: Amorphous Calcium Carbonate and Its Roles in Biomineralization. *Adv. Mater. (Weinheim, Ger.)* **2003**, *15*, 959−970.

(7) Cölfen, H.; Qi, L. M. A Systematic Examination of the Morphogenesis of Calcium Carbonate in the Presence of a Double-Hydrophilic Block Copolymer. *Chem. - Eur. J.* **2001**, *7*, 106−116.

(8) Esumi, K.; Suzuki, A.; Yamahira, A.; Torigoe, K. Role of Poly(Amidoamine) Dendrimers for Preparing Nanoparticles of Gold, Platinum, and Silver. *Langmuir* **2000**, *16*, 2604−2608.

(9) Falini, G.; Albeck, S.; Weiner, S.; Addadi, L. Control of Aragonite or Calcite Polymorphism by Mollusk Shell Macromolecules. *Science* **1996**, *271*, 67−69.

(10) Skrtic, D.; Filipović-Vinceković, N. Inhibition of Calcium Oxalate Crystallization by Sodium Dodecyl Sulphate. *J. Cryst. Growth* **1988**, *88*, 313−320.

(11) Škrtić, D.; Filipović-Vinceković, N.; Füredi-Milhofer, H. Crystallization of Calcium Oxalate in the Presence of Dodecylammonium Chloride. *J. Cryst. Growth* **1991**, *114*, 118−126.

(12) Donners, J. J. J. M.; Heywood, B. R.; Meijer, E. W.; Nolte, R. J. M.; Sommerdijk, N. A. J. M. Control over Calcium Carbonate Phase Formation by Dendrimer/Surfactant Templates. *Chem. - Eur. J.* **2002**, *8*, 2561−2567.

(13) Küther, J.; Seshadri, R.; Knoll, W.; Tremel, W. Templated Growth of Calcite, Vaterite and Aragonite Crystals Onself-Assembled Monolayers of Substituted Alkylthiols on Gold. *J. Mater. Chem.* **1998**, *8*, 641−650.

(14) Mann, S.; Heywood, B. R.; Rajam, S.; Birchall, J. D. Controlled Crystallization of $CaCO_3$ under Stearic Acid Monolayers. *Nature* **2002**, *334*, 692−695.

(15) Walsh, D.; Mann, S. Fabrication of Hollow Porous Shells of Calcium Carbonate from Self-Organizing Media. *Nature* **1995**, *377*, 320−323.

DOI: 10.1021/acsami.5b04679
ACS Appl. Mater. Interfaces 2015, 7, 21115−21129

(16) Sayan, P. Effect of Sodium Oleate on the Agglomeration of Calcium Carbonate. *Cryst. Res. Technol.* **2005**, *40*, 226−232.
(17) Antti, B.-M.; Forssberg, E. Pulp Chemistry in Industrial Mineral Flotation. Studies of Surface Complex on Calcite and Apatite Surfaces Using Ftir Spectroscopy. *Miner. Eng.* **1989**, *2*, 217−227.
(18) Lu, Y.; Drelich, J.; Miller, J. D. Oleate Adsorption at an Apatite Surface Studied by Ex-Situ Ftir Internal Reflection Spectroscopy. *J. Colloid Interface Sci.* **1998**, *202*, 462−476.
(19) Fa, K.; Jiang, T.; Nalaskowski, J.; Miller, J. D. Interaction Forces between a Calcium Dioleate Sphere and Calcite/Fluorite Surfaces and Their Significance in Flotation. *Langmuir* **2003**, *19*, 10523−10530.
(20) Fa, K.; Nguyen, A. V.; Miller, J. D. Interaction of Calcium Dioleate Collector Colloids with Calcite and Fluorite Surfaces as Revealed by Afm Force Measurements and Molecular Dynamics Simulation. *Int. J. Miner. Process.* **2006**, *81*, 166−177.
(21) Somasundaran, P. Adsorption of Starch and Oleate and Interaction between Them on Calcite in Aqueous Solutions. *J. Colloid Interface Sci.* **1969**, *31*, 557−565.
(22) Kawaguchi, H.; Hirai, H.; Sakai, K.; Sera, S.; Nakajima, T.; Ebisawa, Y.; Koyama, K. Crystallization of Inorganic Compounds in Polymer Solutions. Part I: Control of Shape and Form of Calcium Carbonate. *Colloid Polym. Sci.* **1992**, *270*, 1176−1181.
(23) Rieger, J.; Thieme, J.; Schmidt, C. Study of Precipitation Reactions by X-Ray Microscopy: $CaCO_3$ Precipitation and the Effect of Polycarboxylates. *Langmuir* **2000**, *16*, 8300−8305.
(24) Shakkthivel, P.; Sathiyamoorthi, R.; Vasudevan, T. Development of Acrylonitrile Copolymers for Scale Control in Cooling Water Systems. *Desalination* **2004**, *164*, 111−123.
(25) Naka, K.; Huang, S.-C.; Chujo, Y. Formation of Stable Vaterite with Poly(Acrylic Acid) by the Delayed Addition Method. *Langmuir* **2006**, *22*, 7760−7767.
(26) Wang, T. X.; Antonietti, M.; Cölfen, H. Calcite Mesocrystals: "Morphing" Crystals by a Polyelectrolyte. *Chem. - Eur. J.* **2006**, *12*, 5722−5730.
(27) Loy, J. E.; Guo, J.-H.; Severtson, S. Role of Adsorption Fractionation in Determining the $CaCO_3$ Scale Inhibition Performance of Polydisperse Sodium Polyacrylate. *Ind. Eng. Chem. Res.* **2004**, *43*, 1882−1887.
(28) Abdel-Aal, N.; Sawada, K. Inhibition of Adhesion and Precipitation of $CaCO_3$ by Aminopolyphosphonate. *J. Cryst. Growth* **2003**, *256*, 188−200.
(29) Kitano, Y.; Hood, D. W. The Influence of Organic Material on the Polymorphic Crystallization of Calcium Carbonate. *Geochim. Cosmochim. Acta* **1965**, *29*, 29−41.
(30) Meyer, H. J. The Influence of Impurities on the Growth Rate of Calcite. *J. Cryst. Growth* **1984**, *66*, 639−646.
(31) Verch, A.; Gebauer, D.; Antonietti, M.; Cölfen, H. How to Control the Scaling of $CaCO_3$: A "Fingerprinting Technique" to Classify Additives. *Phys. Chem. Chem. Phys.* **2011**, *13*, 16811−16820.
(32) Wada, N.; Yamashita, K.; Umegaki, T. Effects of Carboxylic Acids on Calcite Formation in the Presence of Mg2+Ions. *J. Colloid Interface Sci.* **1999**, *212*, 357−364.
(33) Wheeler, A. P.; George, J. W.; Evans, C. A. Control of Calcium Carbonate Nucleation and Crystal Growth by Soluble Matrix of Oyster Shell. *Science* **1981**, *212*, 1397−1398.
(34) Gebauer, D.; Cölfen, H.; Verch, A.; Antonietti, M. The Multiple Roles of Additives in $CaCO_3$ Crystallization: A Quantitative Case Study. *Adv. Mater. (Weinheim, Ger.)* **2009**, *21*, 435−439.
(35) Iler, R. K. *The Chemistry of Silica: Solubility, Polymerization, Colloid and Surface Properties and Biochemistry of Silica*; John Wiley & Sons: New York, 1979.
(36) Santos, O.; Nylander, T.; Schillén, K.; Paulsson, M.; Trägårdh, C. Effect of Surface and Bulk Properties on the Kinetics and Adsorbed Amount of Whey Proteins onto Steel Surfaces at High Temperature. *J. Food Eng.* **2006**, *73*, 174−189.
(37) Fernandes, C. M.; Senos, A. M. R.; Vieira, M. T. Particle Surface Properties of Stainless Steel-Coated Tungsten Carbide Powders. *Powder Technol.* **2006**, *164*, 124−129.
(38) Hedberg, Y.; Wang, X.; Hedberg, J.; Lundin, M.; Blomberg, E.; Odnevall Wallinder, I. Surface-Protein Interactions on Different Stainless Steel Grades: Effects of Protein Adsorption, Surface Changes and Metal Release. *J. Mater. Sci.: Mater. Med.* **2013**, *24*, 1015−1033.
(39) Landgren, M.; Joensson, B. Determination of the Optical Properties of Si/Sio2 Surfaces by Means of Ellipsometry, Using Different Ambient Media. *J. Phys. Chem.* **1993**, *97*, 1656−1660.
(40) Azzam, R. M. A.; Bashara, N. M. *Ellipsometry and Polarized Light*; Elsevier: North Holland, Amsterdam, 1989.
(41) McCrackin, F. L.; Passaglia, E.; Stromberg, R. R.; Steinberg, H. L. Measurement of the Thickness and Refractive Index of Very Thin Films and the Optical Properties of Surfaces by Ellipsometry. *J. Res. Natl. Bur. Stand., Sect. A* **1963**, *67A* (4), 363−377.
(42) Tiberg, F.; Landgren, M. Characterization of Thin Nonionic Surfactant Films at the Silica/Water Interface by Means of Ellipsometry. *Langmuir* **1993**, *9* (4), 927−932.
(43) de Feijter, J. A.; Benjamins, J.; Veer, F. A. Ellipsometry as a Tool to Study the Adsorption Behavior of Synthetic and Biopolymers at the Air-Water Interface. *Biopolymers* **1978**, *17* (7), 1759−1772.
(44) Svensson, A. V.; Huang, L.; Johnson, E. S.; Nylander, T.; Piculell, L. Surface Deposition and Phase Behavior of Oppositely Charged Polyion/Surfactant Ion Complexes. 1. Cationic Guar Versus Cationic Hydroxyethylcellulose in Mixtures with Anionic Surfactants. *ACS Appl. Mater. Interfaces* **2009**, *1*, 2431−2442.
(45) Svensson, A. V.; Johnson, E. S.; Nylander, T.; Piculell, L. Surface Deposition and Phase Behavior of Oppositely Charged Polyion-Surfactant Ion Complexes. 2. A Means to Deliver Silicone Oil to Hydrophilic Surfaces. *ACS Appl. Mater. Interfaces* **2010**, *2*, 143−156.
(46) Terada, E.; Samoshina, Y.; Nylander, T.; Lindman, B. Adsorption of Cationic Cellulose Derivatives/Anionic Surfactant Complexes onto Solid Surfaces. I. Silica Surfaces. *Langmuir* **2004**, *20*, 1753−1762.
(47) Klevens, H. B. Structure and Aggregation in Dilute Solutions of Surface Active Agents. *J. Am. Oil Chem. Soc.* **1953**, *30*, 74−80.
(48) Beneventi, D.; Carré, B.; Gandini, A. Precipitation and Solubility of Calcium Soaps in Basic Aqueous Media. *J. Colloid Interface Sci.* **2001**, *237*, 142−144.
(49) Barhoum, A.; El-Sheikh, S. M.; Morsy, F.; El-Sherbiny, S.; Reniers, F.; Dufour, T.; Delplancke, M. P.; Van Assche, G.; Rahier, H. Preparation and Characterization of Ultra-Hydrophobic Calcium Carbonate Nanoparticles. *IOP Conf. Ser.: Mater. Sci. Eng.* **2014**, *64*, 012037.
(50) Sheng, Y.; Zhou, B.; Wang, C. Y.; Zhao, X.; Deng, Y. H.; Wang, Z. C. In Situ Preparation of Hydrophobic $CaCO_3$ in the Presence of Sodium Oleate. *Appl. Surf. Sci.* **2006**, *253*, 1983−1987.
(51) Wang, H.; Alfredsson, V.; Tropsch, J.; Ettl, R.; Nylander, T. Formation of $CaCO_3$ Deposits on Hard Surfaces—Effect of Bulk Solution Conditions and Surface Properties. *ACS Appl. Mater. Interfaces* **2013**, *5*, 4035−4045.
(52) Wucher, B.; Yue, W.; Kulak, A. N.; Meldrum, F. C. Designer Crystals: Single Crystals with Complex Morphologies. *Chem. Mater.* **2007**, *19*, 1111−1119.
(53) Liu, X.; Dedinaite, A.; Nylander, T.; Dabkowska, A. P.; Skoda, M.; Makuska, R.; Claesson, P. M. Association of Anionic Surfactant and Physisorbed Branched Brush Layers Probed by Neutron and Optical Reflectometry. *J. Colloid Interface Sci.* **2015**, *440*, 245−252.
(54) Samoshina, Y.; Nylander, T.; Shubin, V.; Bauer, R.; Eskilsson, K. Equilibrium Aspects of Polycation Adsorption on Silica Surface: How the Adsorbed Layer Responds to Changes in Bulk Solution. *Langmuir* **2005**, *21* (13), 5872−5881.
(55) Jiang, Y.; Gong, H.; Grzywa, M.; Volkmer, D.; Gower, L.; Cölfen, H. Microdomain Transformations in Mosaic Mesocrystal Thin Films. *Adv. Funct. Mater.* **2013**, *23*, 1547−1555.
(56) Kellermeier, M.; Gebauer, D.; Melero-García, E.; Drechsler, M.; Talmon, Y.; Kienle, L.; Cölfen, H.; García-Ruiz, J. M.; Kunz, W. Colloidal Stabilization of Calcium Carbonate Prenucleation Clusters with Silica. *Adv. Funct. Mater.* **2012**, *22*, 4301−4311.
(57) Sinn, C. G.; Dimova, R.; Antonietti, M. Isothermal Titration Calorimetry of the Polyelectrolyte/Water Interaction and Binding of

DOI: 10.1021/acsami.5b04679
ACS Appl. Mater. Interfaces 2015, 7, 21115−21129

Ca2+: Effects Determining the Quality of Polymeric Scale Inhibitors. *Macromolecules* **2004**, *37*, 3444−3450.
(58) Clauzel, M.; Johnson, E. S.; Nylander, T.; Panandiker, R. K.; Sivik, M. R.; Piculell, L. Surface Deposition and Phase Behavior of Oppositely Charged Polyion-Surfactant Ion Complexes. Delivery of Silicone Oil Emulsions to Hydrophobic and Hydrophilic Surfaces. *ACS Appl. Mater. Interfaces* **2011**, *3*, 2451−2462.
(59) Mohr, A.; Nylander, T.; Piculell, L.; Lindman, B.; Boyko, V.; Bartels, F. W.; Liu, Y.; Kurkal-Siebert, V. Mixtures of Cationic Copolymers and Oppositely Charged Surfactants: Effect of Polymer Charge Density and Ionic Strength on the Adsorption Behavior at the Silica−Aqueous Interface. *ACS Appl. Mater. Interfaces* **2012**, *4*, 1500−1511.
(60) Nylander, T.; Samoshina, Y.; Lindman, B. Formation of Polyelectrolyte-Surfactant Complexes on Surfaces. *Adv. Colloid Interface Sci.* **2006**, *123−126*, 105−123.
(61) Datta, S.; Conlisk, A. T.; Li, H. F.; Yoda, M. Effect of Divalent Ions on Electroosmotic Flow in Microchannels. *Mech. Res. Commun.* **2009**, *36*, 65−74.

DOI: 10.1021/acsami.5b04679
ACS Appl. Mater. Interfaces 2015, 7, 21115−21129